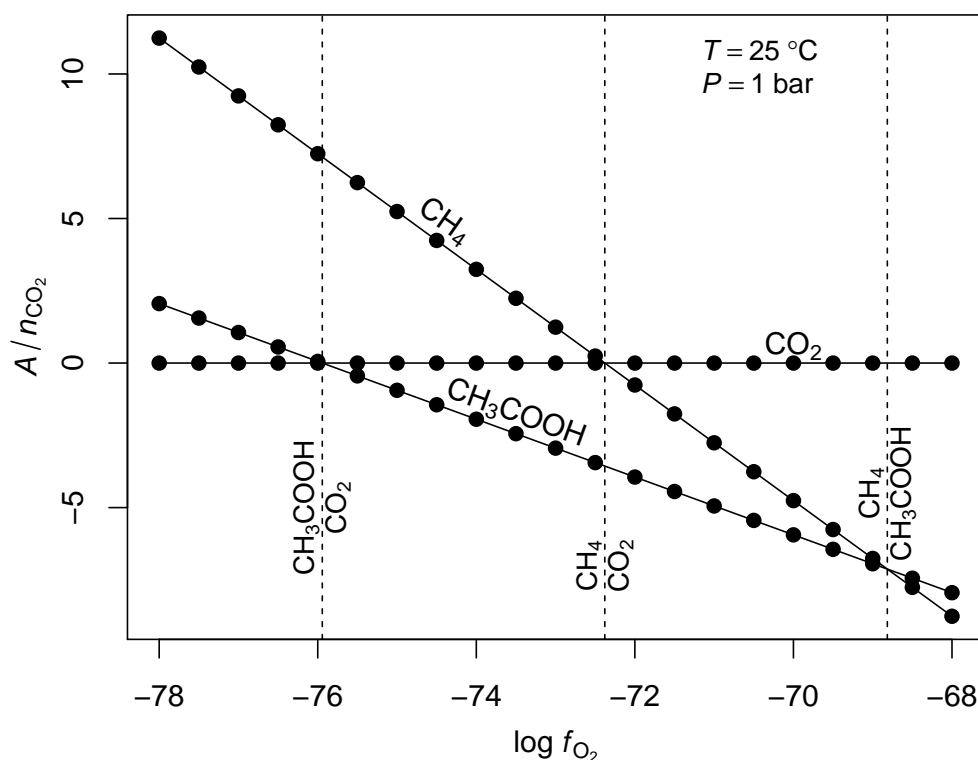


# Supplementary Material: CHNOSZ: Thermodynamic Calculations and Diagrams for Geochemistry

## 1 SUPPLEMENTAL FIGURES

The code used to make all of these figures is available ([Dick, 2019](#)).



**Figure S1.** Comparison of equilibrium constant and maximum affinity methods. Vertical dashed lines represent equilibrium  $\log f_{\text{O}_2}$  values calculated from equilibrium constants of reactions between two species balanced on carbon. Evenly-spaced points on the  $x$  axis ( $\log f_{\text{O}_2}$ ) have  $y$  values representing the affinities of reactions to form a single species divided by the number of  $\text{CO}_2$  in the reaction. Solid lines drawn through the points intersect at the positions of the vertical lines. The highest affinity at any location on the  $x$  axis indicates the most stable species. Activities of aqueous species other than  $\text{H}_2\text{O}$  are set to  $10^{-3}$ .

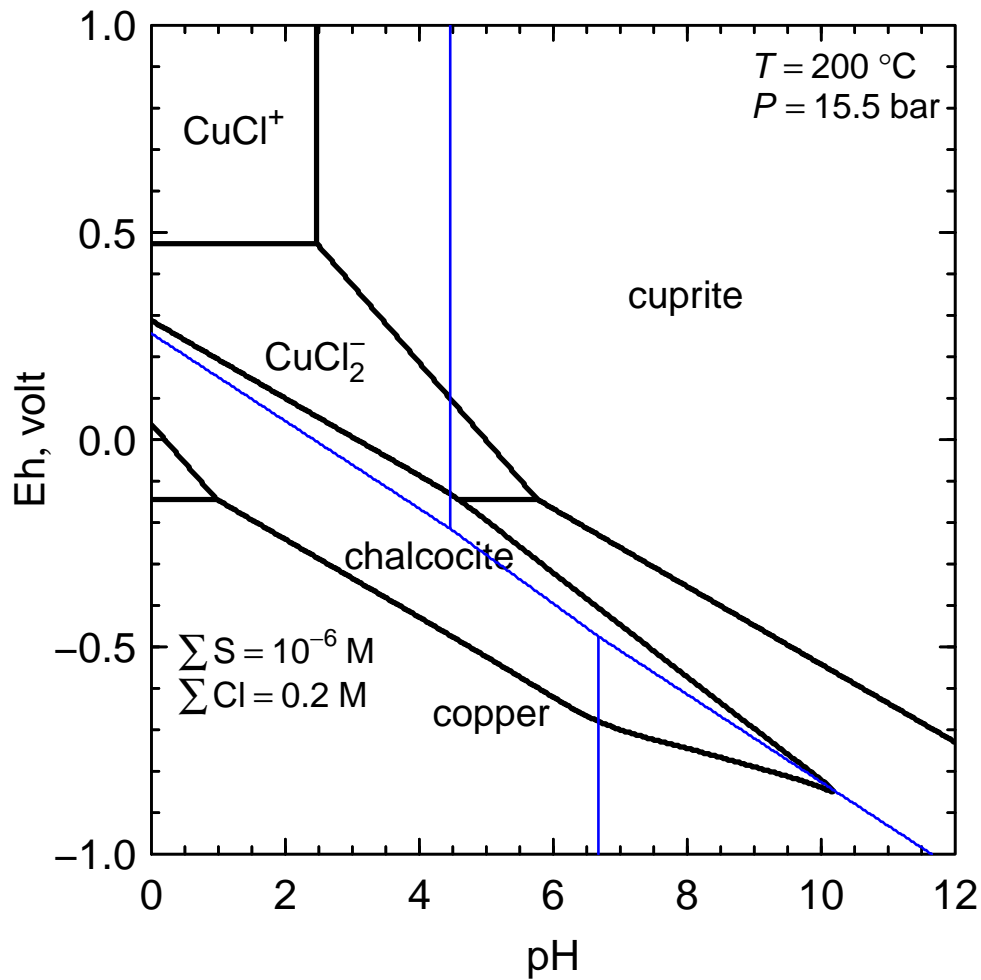


**Figure S2.** Similar to **Figure 4B** in the main text, with modifications to reproduce Figure 5a of [Caporuscio et al. \(2017\)](#). The modifications are 1) activating the SLOP98 optional data file in order to load data for aqueous Cu(I) species ([Sverjensky et al., 1997](#)) that have since been superseded in CHNOSZ, and 2) changing the balancing coefficients to unity. Setting the balancing coefficients to unity is not recommended for most calculations.

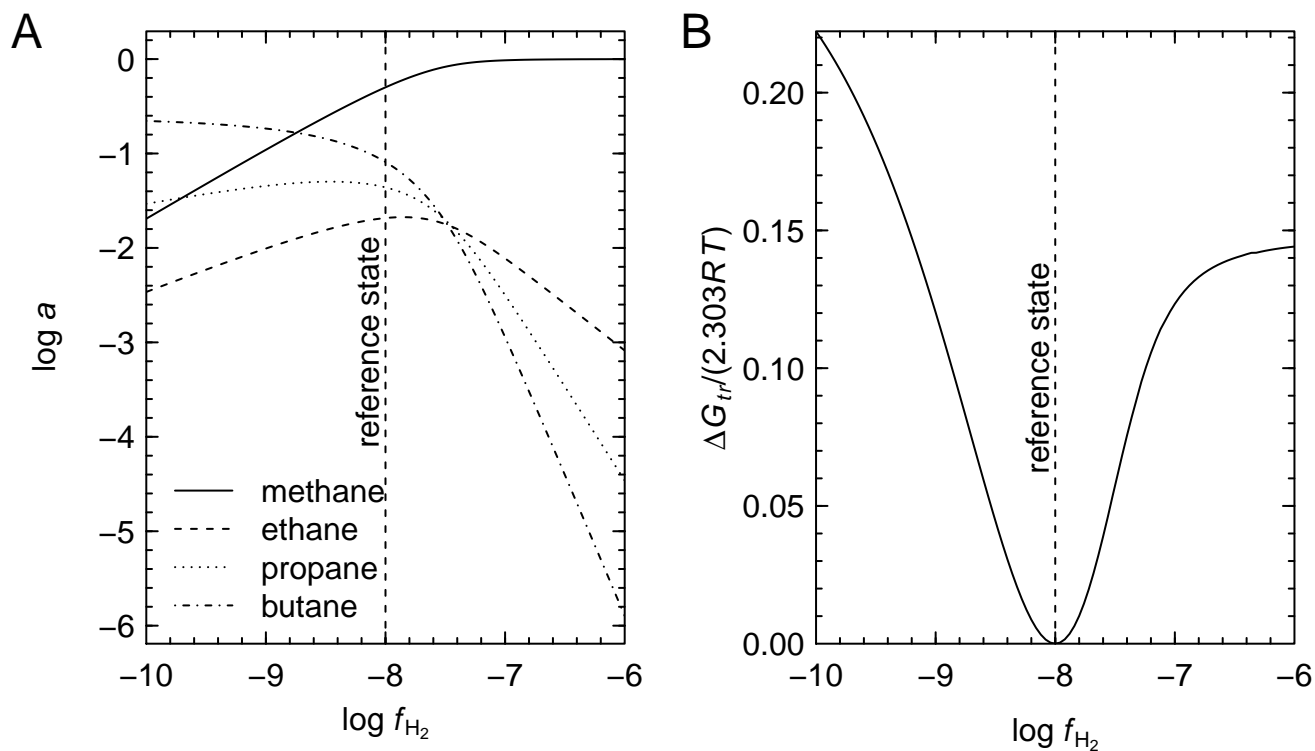


**Figure S3.** Calculation of the Gibbs energy of transformation of a chemical system ( $\Delta G_{tr}$ ) using equations given in [Dick and Shock \(2013\)](#). **(A)** Equilibrium activities of a hypothetical system of C<sub>1</sub>–C<sub>4</sub> n-alkanes as a function of  $\log f_{\text{H}_2}$  at 25 °C and 1 bar and total activity of C equal to 1. For the purposes of this example, the equilibrium activities at  $\log f_{\text{H}_2} = -8$  are chosen as the reference state, and the equilibrium activities at any given  $\log f_{\text{H}_2}$  are used as “observed” activities. **(B)** Dimensionless values of Gibbs energy of transformation ( $\Delta G_{tr}/(2.303RT)$ ) as a function of  $\log f_{\text{H}_2}$ . Note that  $\Delta G_{tr} = 0$  only at  $\log f_{\text{H}_2} = -8$ , where the reference and observed activities are identical; at all other conditions,  $\Delta G_{tr} > 0$ , representing the energetic distance from equilibrium of the system with the observed activities.

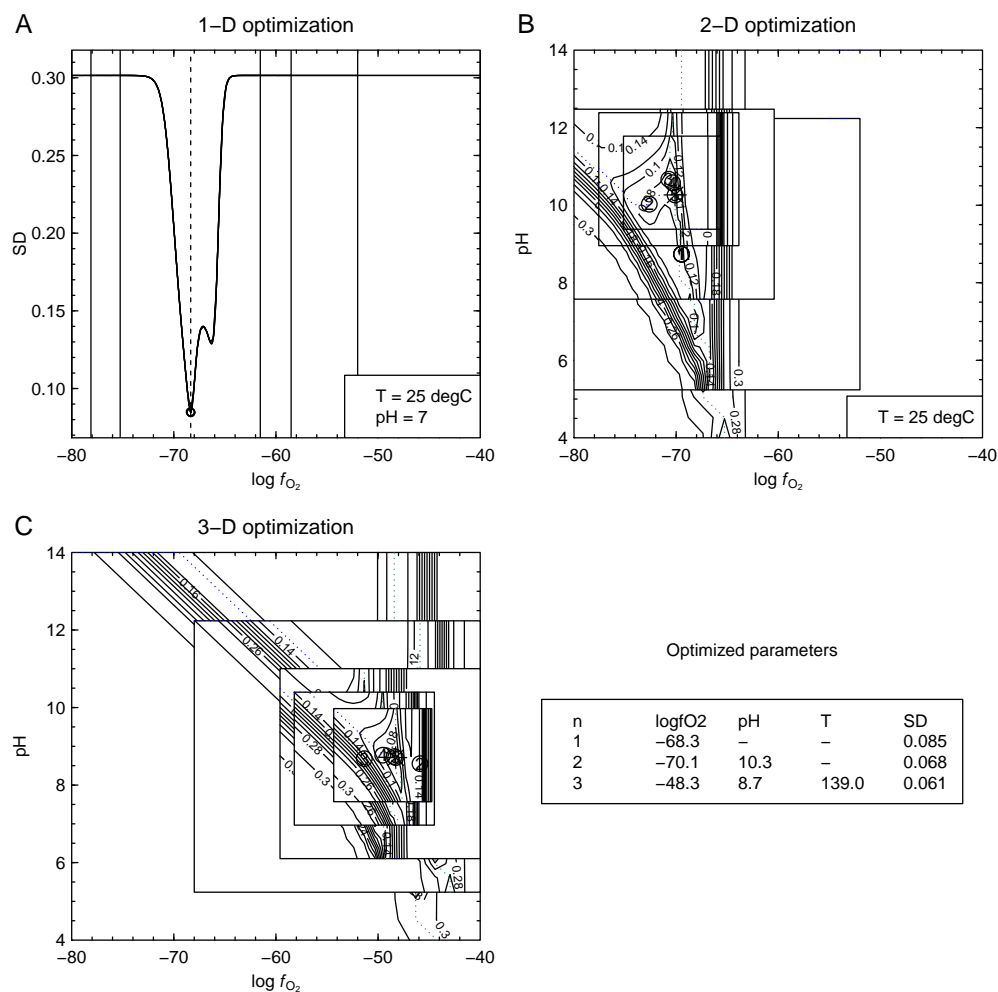


**Figure S4.** Optimization of system parameters using the *findit* function. Equilibrium activities are calculated for 11 aqueous sulfur species ( $\text{H}_2\text{S}$ ,  $\text{S}_2^{-2}$ ,  $\text{S}_3^{-2}$ ,  $\text{S}_2\text{O}_3^{-2}$ ,  $\text{S}_2\text{O}_4^{-2}$ ,  $\text{S}_3\text{O}_6^{-2}$ ,  $\text{S}_5\text{O}_6^{-2}$ ,  $\text{S}_2\text{O}_6^{-2}$ ,  $\text{HSO}_3^-$ ,  $\text{SO}_2$ ,  $\text{HSO}_4^-$ ) (cf. Figure 5 of Seewald, 1996). The standard deviation (SD) of the logarithms of activities is used as the objective function for the optimization. **(A)** Temperature and pH are held constant, and  $\log f_{\text{O}_2}$  is optimized. The horizontal lines show the decreasing ranges of  $\log f_{\text{O}_2}$  used in successive iterations; the dashed line and symbol show the optimal  $\log f_{\text{O}_2}$  and minimum SD. **(B)** Temperature is held constant, and  $\log f_{\text{O}_2}$  and pH are optimized. The contours show the values of SD and the boxes show the decreasing ranges of  $\log f_{\text{O}_2}$  and pH in successive iterations. Numbered circles indicate the optimal values after each iteration; the star symbol indicates the values after the last iteration. **(C)** Temperature,  $\log f_{\text{O}_2}$  and pH are optimized. The boxes show the decreasing ranges of  $\log f_{\text{O}_2}$  and pH in successive iterations. Although the range of temperature also decreases, it is not possible to plot it on this diagram; however, its effect is visible in the shifted positions of the SD contours after each iteration. The table gives the optimized parameters; the SD decreases with increasing number of variables (n).

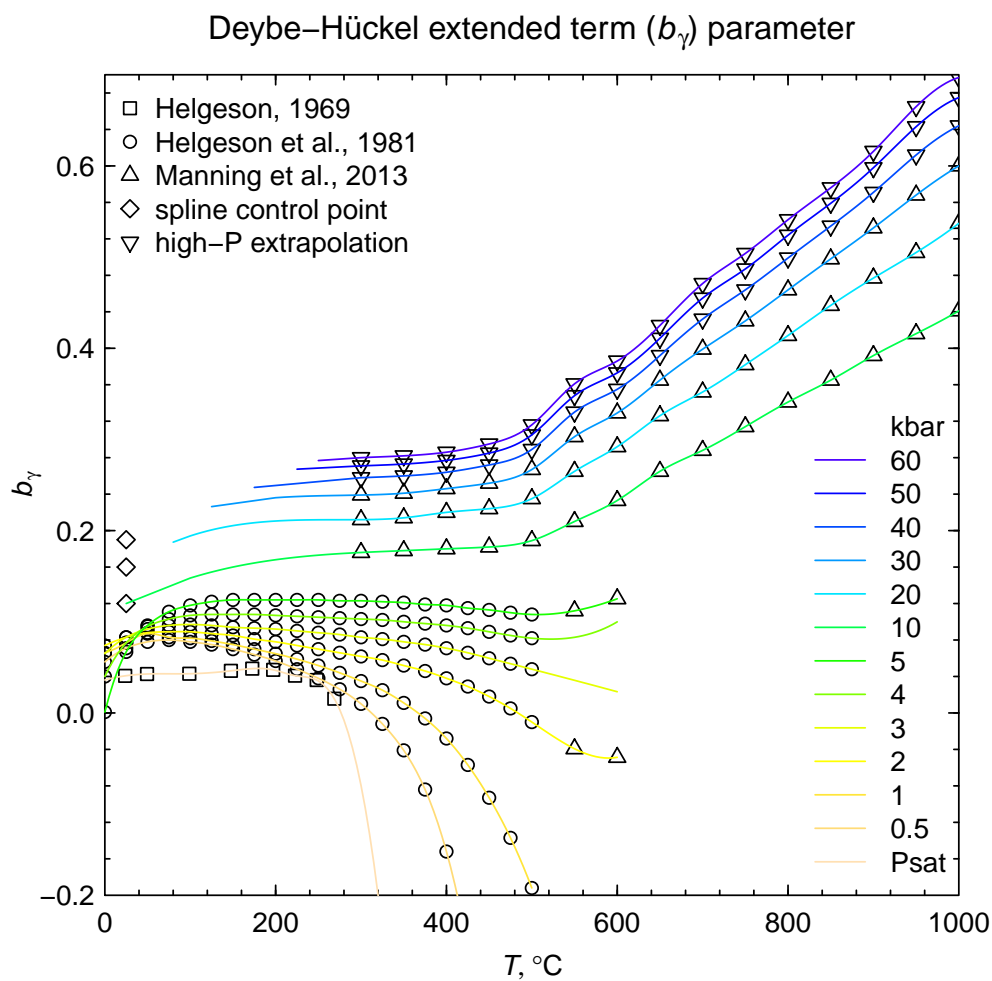


**Figure S5.** Values of the extended-term parameter in the Debye-Hückel equation. Points represent values taken from the literature (Helgeson, 1969; Helgeson et al., 1981; Manning et al., 2013), except for ( $\diamond$ ) control points used for spline extrapolation of 10–30 kbar values to lower temperatures and ( $\nabla$ ) points extrapolated to 60 kbar by fitting a geometric progression to the 10, 20 and 30 kbar values of Manning et al. (2013). Lines represent the values used in CHNOSZ with the “bgamma” option.

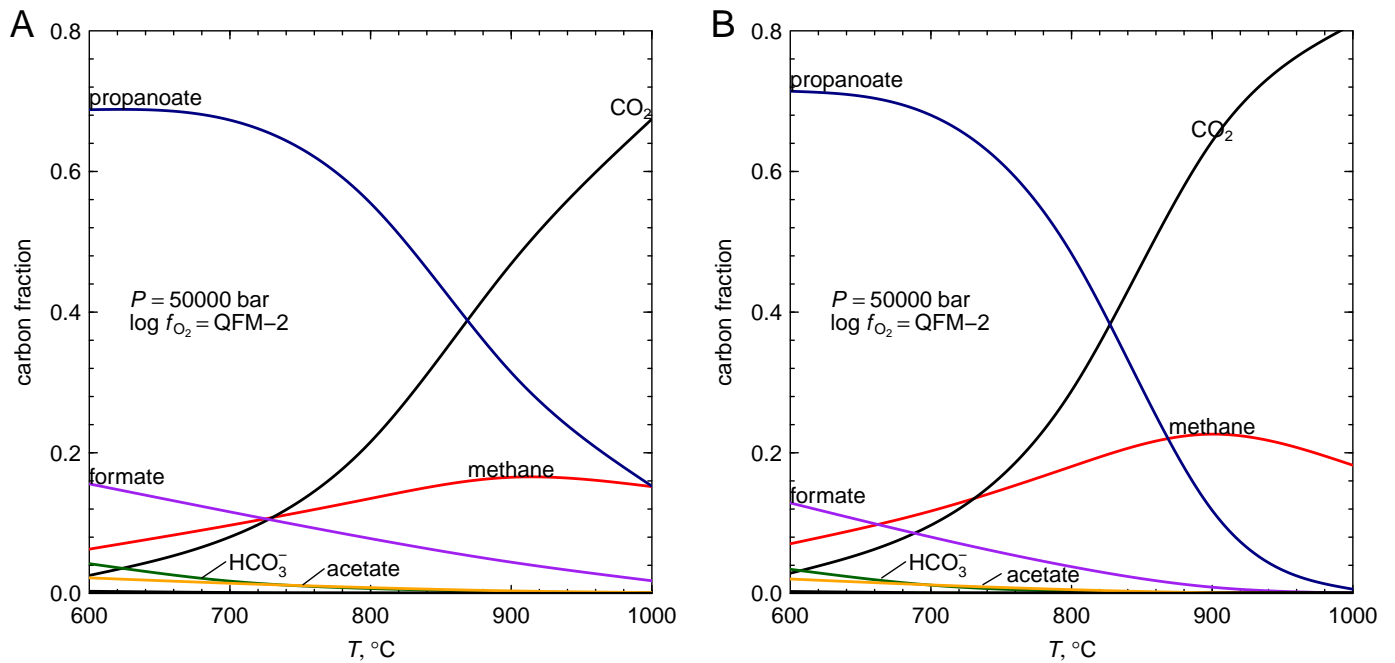


**Figure S6.** (A) Diagram constructed as in **Figure 6** in the main text, but excluding the updated HKF parameters of acetate in the DEW spreadsheet. The presence of a small amount of acetate is consistent with the EQ3NR output in the Supplementary Information of [Sverjensky et al. \(2014\)](#). (B) Diagram constructed as in (A), but using activity coefficients calculated with the “bgamma” setting, which estimates the extended term parameter in the Debye-Hückel equation based on extrapolations from [Manning et al. \(2013\)](#) (see **Figure S5**).

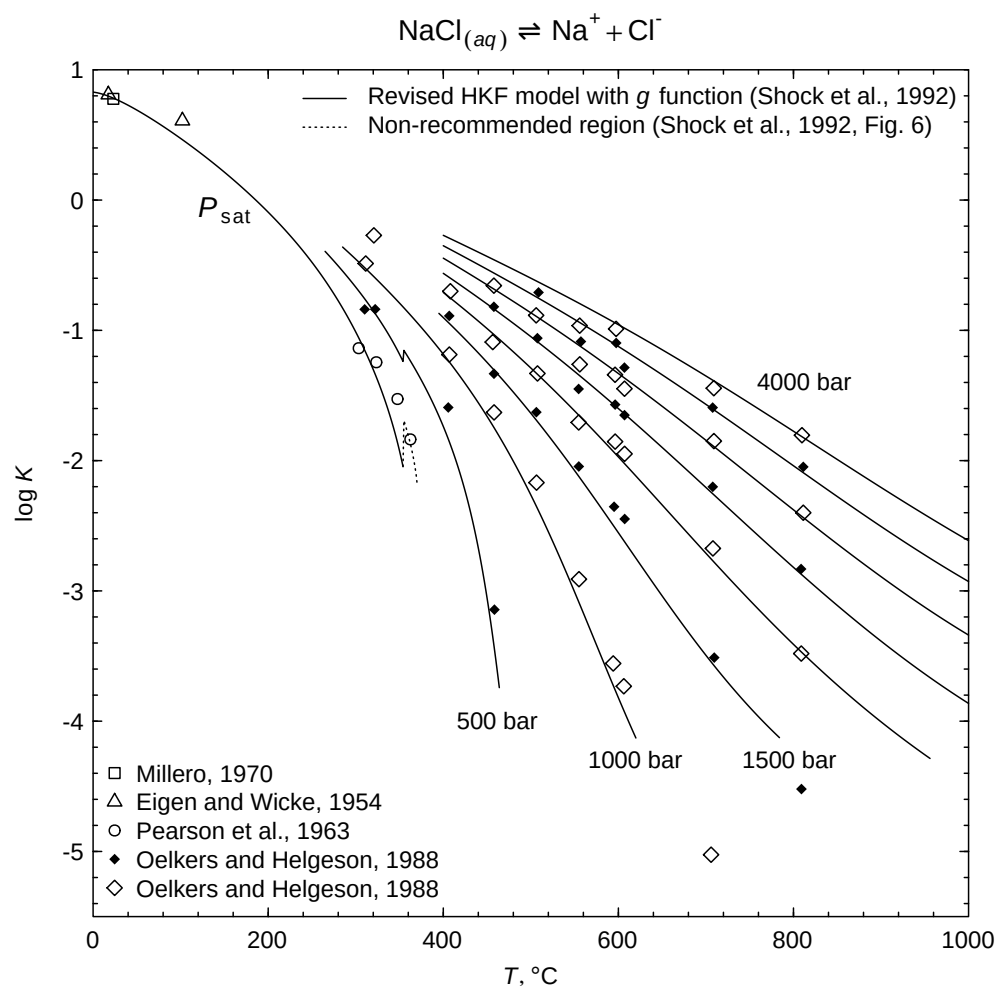


**Figure S7.** The output of demo ("NaCl"), which is based on Figure 1 of [Shock et al. \(1992\)](#). The breaks in the curves at  $P_{\text{sat}}$  and 500 bar occur at the 355 °C boundary of region II for applicability of the  $g$  function ([Shock et al., 1992](#), Figure 6). SUPCRT92 ([Johnson et al., 1992](#)) prohibits calculations above 350 °C at  $P_{\text{sat}}$ , but it can be used to confirm the presence of the discontinuity in the 500 bar curve.

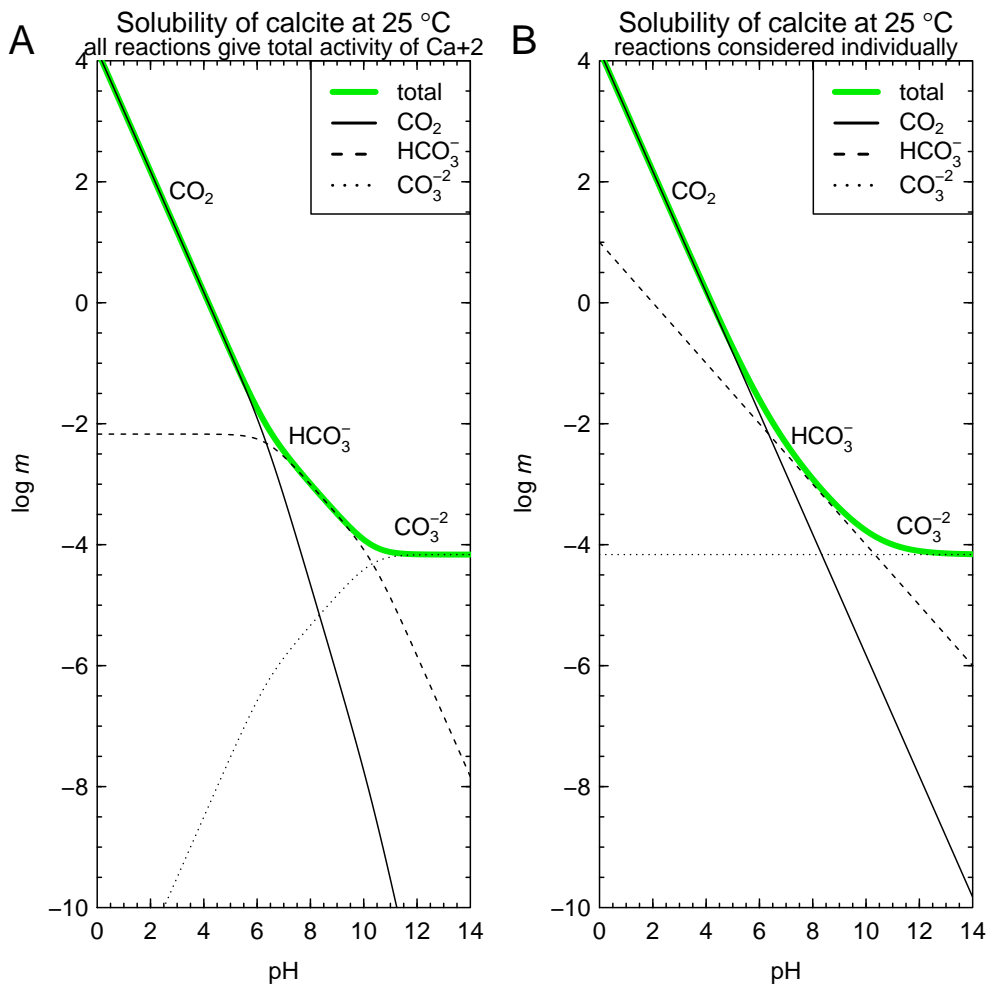


**Figure S8.** Two calculations for the solubility of calcite in a closed system at 25 °C, illustrating the effects of the “dissociation” argument of the `solubility` function. Both plots show the distribution of different carbonate species (carbonic acid, bicarbonate, carbonate) that form as a result of dissolution and dissociation of CaCO<sub>3</sub>. In **(A)**, speciation of carbonate is calculated for the total concentration of Ca<sup>+2</sup> in the system considering all reactions; in **(B)**, the concentration of Ca<sup>+2</sup> is calculated independently for each reaction. The diagram on the left is recommended (see inset of Figure 7.9 of [Stumm and Morgan, 1996](#)) but a diagram like the one on the right has also been previously published ([Manning et al., 2013](#)).

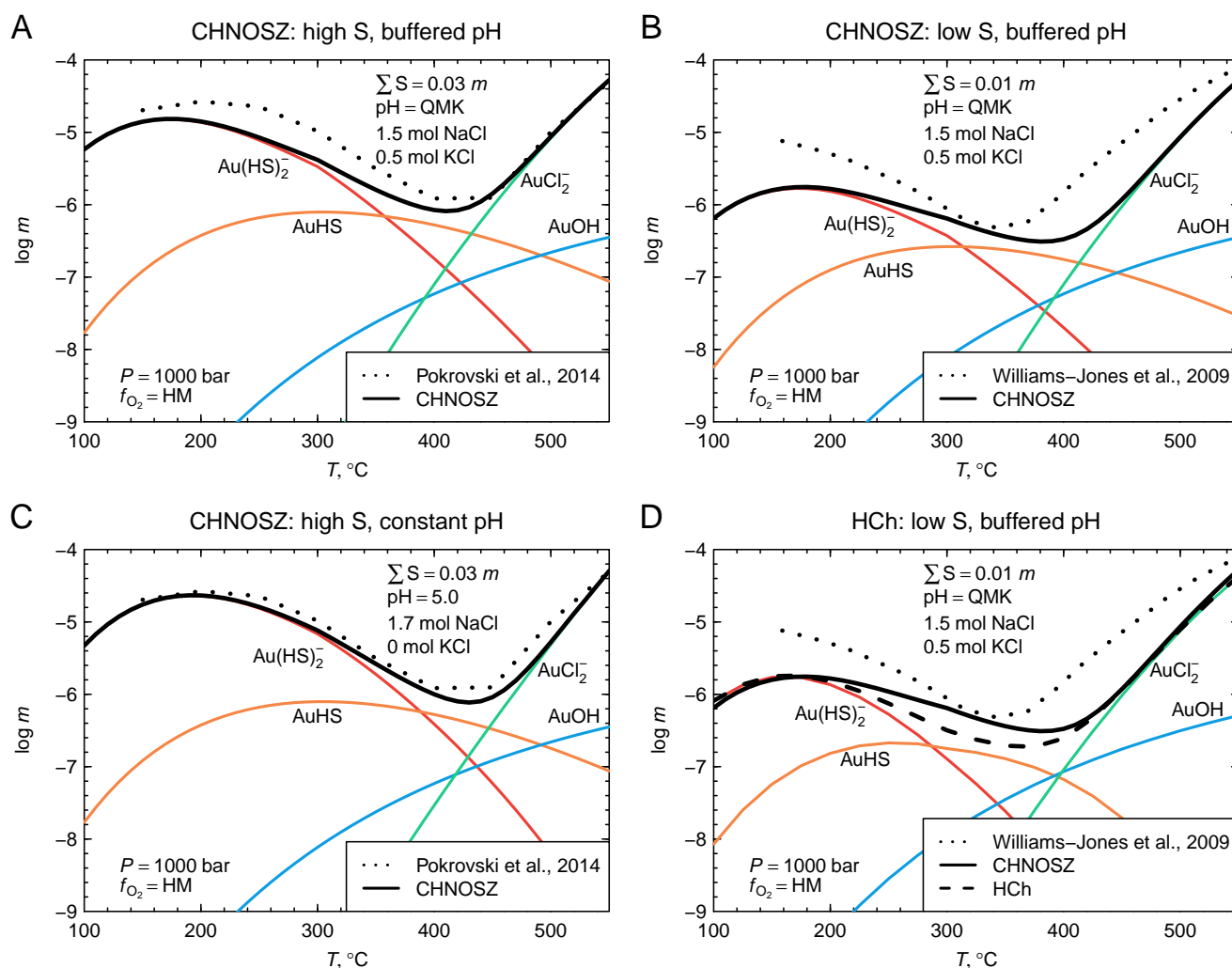


**Figure S9.** Comparison of gold solubility calculated using (A–C) CHNOSZ and (D) HCh (Shvarov and Bastrakov, 1999). All calculations use the hematite-magnetite (HM) buffer for  $f_{\text{O}_2}$  and quartz-muscovite-K-feldspar (QMK) buffer for pH, except (C) constant pH = 5. Total S is (A, C) 0.03 m, corresponding to 0.1 wt% S, as in Figure 8a of Pokrovski et al. (2014), or (B, D) 0.01 m, as in Figure 2A of Williams-Jones et al. (2009). All calculations were made for 1.5 mol NaCl and 0.5 mol KCl, as in Figure 2A of Williams-Jones et al. (2009), except (C) 1.7 mol NaCl, corresponding to 10 wt%, as in Figure 8a of Pokrovski et al. (2014). Note that a whole-solution speciation model is not available in CHNOSZ; instead, the ionic strength of the solution is estimated from the reaction  $\text{NaCl}(\text{aq}) = \text{Na}^+ + \text{Cl}^-$  assuming 2 mol NaCl, then the molality of  $\text{K}^+$  given 0.5 mol KCl is computed from the reaction  $\text{KCl}(\text{aq}) = \text{K}^+ + \text{Cl}^-$  (using the ionic strength computed for 2 mol NaCl). In CHNOSZ, setting the molality of the basis species  $\text{H}_2\text{S}$  gives a close approximation to total S, because the S-bearing Au complexes are formed at much lower concentrations (maximum ca.  $2 \times 10^{-6}$  m). In order to use the same thermodynamic data in the calculations, the thermodynamic database shipped with HCh version 3.7 was updated with data for  $\text{KCl}(\text{aq})$  and  $\text{NaCl}(\text{aq})$  from Sverjensky et al. (1997), data for  $\text{AuOH}$  and  $\text{AuCl}_2^-$  from Akinfiev and Zotov (2001), and data for  $\text{AuHS}$  and  $\text{Au}(\text{HS})_2^-$  from Akinfiev and Zotov (2010), and the CHNOSZ calculations were set up to use mineral data from Helgeson et al. (1978). See Section 3 for the HCh output file at 300 °C.

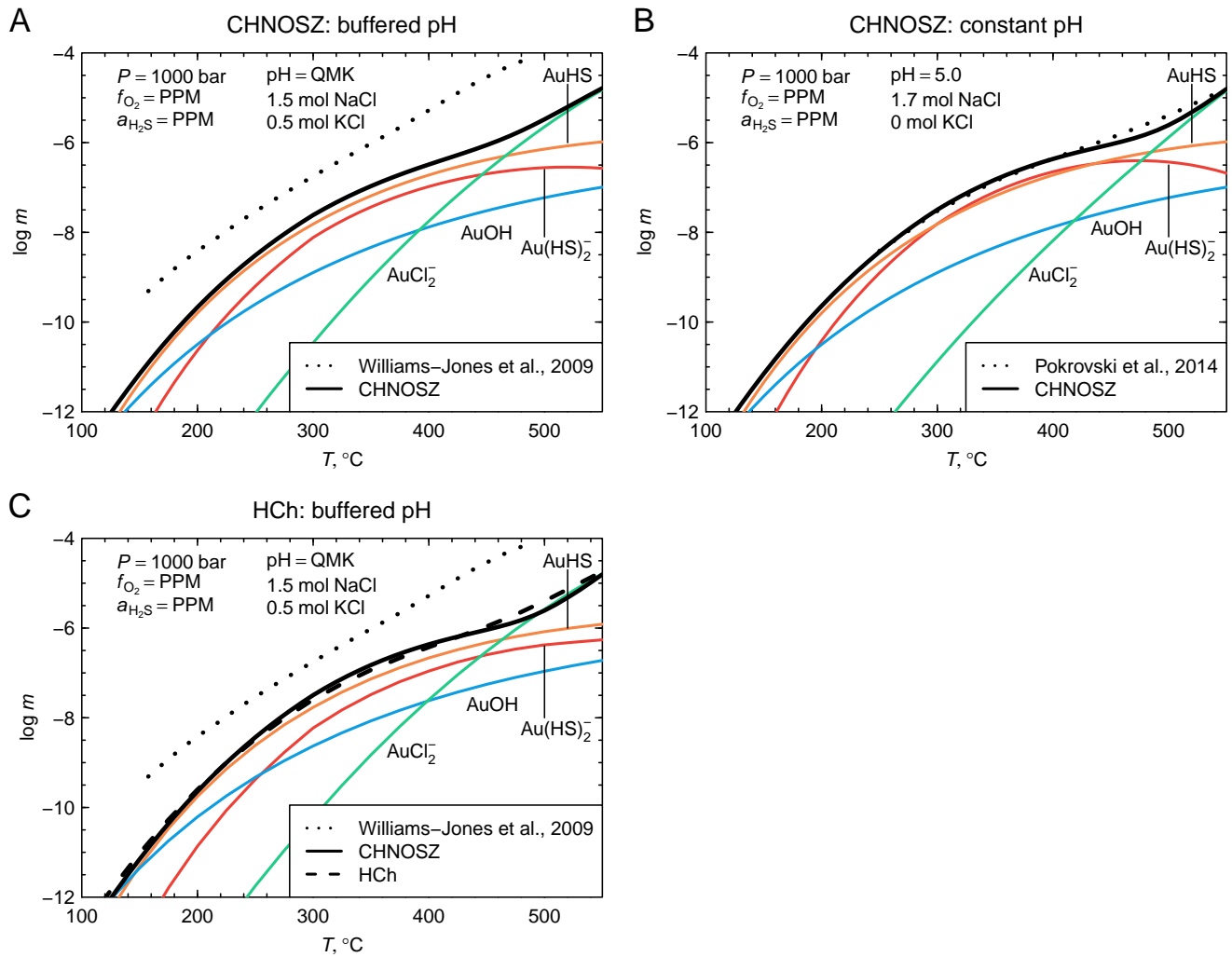


**Figure S10.** Comparison of gold solubility calculated using (A–B) CHNOSZ and (C) HCh (Shvarov and Bastrakov, 1999). Calculations were made using the pyrite-pyrrhotite-magnetite (PPM) buffer for  $f_{\text{O}_2}$  and  $a_{\text{H}_2\text{S}}$  and quartz-muscovite-K-feldspar (QMK) buffer for pH, with 1.5 mol NaCl and 0.5 mol KCl, as in Figure 2B of Williams-Jones et al. (2009), except (B) constant pH = 5 and 1.7 mol NaCl, corresponding to 10 wt%, as in Figure 8a of Pokrovski et al. (2014). See Figure S9 for more notes on the calculations and Section 3 for the HCh output file at 300 °C.

## 2 APPENDIX: DESCRIPTION OF THE MAXIMUM AFFINITY METHOD

Equal-activity lines on diagrams can be easily calculated by hand using equilibrium constants for reactions between the two species. However, for a grid-based calculation with the computer it is more convenient to identify the most stable species at any point on the diagram as the formation reaction having the maximum affinity.

A more technical description of the method is that given equal, non-equilibrium reference activities of the species of interest, the formation reaction with the most positive affinity indicates the species that would have the highest activity in the equilibrium distribution, where the affinities become equal. The calculations described below for a hypothetical system composed of aqueous CH<sub>4</sub>, CO<sub>2</sub>, and CH<sub>3</sub>COOH (acetic acid) show that graphical methods based on equilibrium constants ( $\log K$ ) and maximum affinity (MAM) produce equivalent diagrams.

### 2.1 $\log K$ method

What is the  $\log f_{\text{O}_2}$  for equal activities of CH<sub>4</sub> and CO<sub>2</sub> at equilibrium? The solution using the  $\log K$  method begins with writing a reaction balanced on carbon,



for which, at equilibrium,  $\log K_1 = \log a_{\text{CH}_4} + 2 \log f_{\text{O}_2} - 2 \log a_{\text{H}_2\text{O}} - \log a_{\text{CO}_2}$ . At 25 °C and 1 bar, we have  $\log K = -144.76$  (rounded to two decimal places). Letting  $\log a_{\text{H}_2\text{O}} = 0$  and  $\log a_{\text{CH}_4} = \log a_{\text{CO}_2}$ , we get  $\log f_{\text{O}_2} = -72.38$ .

Similarly, it can be shown that  $\log f_{\text{O}_2} = -75.94$  for activities of CO<sub>2</sub> and CH<sub>3</sub>COOH both equal to 10<sup>-3</sup>, and  $\log f_{\text{O}_2} = -68.82$  for activities of CH<sub>4</sub> and CH<sub>3</sub>COOH both equal to 10<sup>-3</sup>. For the latter case, we can write



which, at equilibrium, gives  $\log K = \log a_{\text{CH}_3\text{COOH}} + 2 \log a_{\text{H}_2\text{O}} - 2 \log f_{\text{O}_2} - 2 \log a_{\text{CH}_4}$ . This equation shows that, because of the unequal reaction coefficients on CH<sub>4</sub> and CH<sub>3</sub>COOH, it does not suffice to specify “equal activities”. Instead, obtaining a value for  $\log f_{\text{O}_2}$  depends on a statement like “activities equal to  $a$ ”; here, we choose  $a = 10^{-3}$ .

### 2.2 Maximum affinity method

Turning to the MAM, how can we find the  $\log f_{\text{O}_2}$  that is compatible with  $\log a_{\text{CH}_4} = \log a_{\text{CH}_3\text{COOH}} = -3$ ? First, let us choose the basis species to be CO<sub>2</sub>, O<sub>2</sub> and H<sub>2</sub>O. Accordingly, Reaction S1 represents the formation of CH<sub>4</sub> from the basis species, while



represents the formation of CH<sub>3</sub>COOH from the basis species. Starting with  $\log f_{\text{O}_2} = -68.816$  (the solution found above) and  $\log a_{\text{CO}_2} = -3$  (a reference value), we find that  $\mathbf{A}_1 = \log(K_1/Q_1) = -7.13$  and  $\mathbf{A}_2 = \log(K_2/Q_2) = -14.25$ . The bold symbol  $\mathbf{A}$  is used here to represent the dimensionless value of chemical affinity ( $A$ ), such that  $\mathbf{A} = A/(2.303RT) = \log(K/Q)$ , where  $R$  is the gas constant,  $T$  is temperature in Kelvin, and  $Q$  is the activity quotient for the species in the reaction.

To apply the balancing constraint in the MAM, the affinity of each of the formation reactions is divided by the stoichiometric coefficient of  $\text{CO}_2$  in the reaction, giving  $A_1/n_{\text{CO}_2,1} = -7.13$  and  $A_2/n_{\text{CO}_2,2} = -7.13$ . These normalized affinities represent the per-carbon potential for formation of the species, and the equal values indicate that  $\text{CH}_4$  and  $\text{CH}_3\text{COOH}$  with activities of  $10^{-3}$  are in equilibrium at  $\log f_{\text{O}_2} = -68.816$ .

In **Figure S1** the values of  $\log f_{\text{O}_2}$  calculated using the  $\log K$  method (dashed vertical lines) are compared with the normalized (per-carbon) affinities of the formation reactions at  $\log f_{\text{O}_2}$  intervals, as used in the MAM. To complete the MAM calculation, a third reaction, representing the formation of  $\text{CO}_2$  from the basis species, is needed:



This reaction has  $A_3 = 0$ , as shown by the horizontal line in **Figure S1**.

### 2.3 Comparison of the methods

The reactions used in the  $\log K$  method are transformation reactions that can be combined with “activities of species equal to” statements to solve for  $\log f_{\text{O}_2}$  or other variables of interest. In contrast, the reactions considered within the MAM are formation reactions from basis species. Rather than solve for  $\log f_{\text{O}_2}$ , the normalized affinities (divided by the balancing coefficients) are computed at  $\log f_{\text{O}_2}$  intervals, which are plotted as points in **Figure S1**. The lines connecting the points represent affinities that could be calculated by decreasing the interval size; it is apparent that any two of these lines cross at a  $\log f_{\text{O}_2}$  corresponding to equal activities calculated from the  $\log K$  of the corresponding reaction (dashed vertical lines). Note that the reference value chosen for the activity of the conserved basis species shifts all of the normalized affinities equally, and therefore has no effect on the calculated equilibrium values of  $\log f_{\text{O}_2}$ . The MAM also reveals the relative instability of  $\text{CH}_3\text{COOH}$  in this system: its normalized affinity is always below the maximum. This result is consistent with the outward positions of  $\text{CH}_3\text{COOH}$  in its reactions with  $\text{CH}_4$  and  $\text{CO}_2$  as judged by the  $\log K$  method.

### 3 SAMPLE HCH OUTPUT FILES

Bold values indicate species whose concentrations are plotted in **Figure S9D** and **Figure S10C**.

FigS7	FigS8
=====	=====
Temperature 573.15 K (300.00 C)	Temperature 573.15 K (300.00 C)
Total pressure 1000 bar	Total pressure 1000 bar
Au-HM	Au-PPM
Total system composition	Total system composition
H2O 1.000000E+00 kg	H2O 1.000000E+00 kg
SiO2 1.000000E+00 kg	SiO2 1.000000E+00 kg
KAlSi3O8 1.000000E+00 kg	KAlSi3O8 1.000000E+00 kg
KAl3Si3O12H2 1.000000E+00 kg	KAl3Si3O12H2 1.000000E+00 kg
Fe2O3 1.000000E+00 kg	Fe3O4 1.000000E+00 kg
Fe3O4 1.000000E+00 kg	FeS2 1.000000E+00 kg
Au 1.000000E+00 kg	FeS 1.000000E+00 kg
KCl 5.000000E-01 mol	Au 1.000000E+00 kg
NaCl 1.500000E+00 mol	KCl 5.000000E-01 mol
H2S 1.000000E-02 mol	NaCl 1.500000E+00 mol
	H2S 0.000000E+00 mol
===== Individual phases =====	===== Individual phases =====
1 5.077005E+00 16.671% Gold	1 5.077005E+00 14.287% Gold
2 1.666204E+01 16.690% Quartz	2 1.662969E+01 14.276% Quartz
3 6.196249E+00 16.496% Hematite	3 4.319488E+00 14.289% Magnetite
4 4.362786E+00 16.840% Magnetite	4 6.538591E+00 11.208% Pyrite
5 2.515825E+00 16.705% Muscovite	5 1.496515E+01 17.364% Pyrrhotite
6 3.577218E+00 16.598% Microcline	6 2.510434E+00 14.286% Muscovite
Total 3.839112E+01 (mol)	7 3.593392E+00 14.289% Microcline
	Total 5.363375E+01 (mol)
Bulk composition (mol)	Bulk composition (mol)
Al 1.112469E+01	Al 1.112469E+01
Au 5.077005E+00	Au 5.077005E+00
Cl --	Cl --
Fe 2.548086E+01	Fe 3.266638E+01
H 5.031650E+00	H 5.020867E+00
K 6.093043E+00	K 6.103825E+00
Na --	Na --
O 1.281716E+02	O 1.094097E+02
S --	S 2.804233E+01
Si 3.494117E+01	Si 3.494117E+01
Total 2.159200E+02	Total 2.323859E+02

===== Aqueous solution =====				===== Aqueous solution =====			
0	9.408776E-01*	1.00000*	H2O	0	9.411136E-01*	1.00000*	H2O
1	3.083214E-05	0.56153	H+	1	3.037019E-05	0.56183	H+
2	4.998763E-06	0.34060	OH-	2	5.066577E-06	0.34106	OH-
3	6.717246E-06	0.39658	H3SiO4-	3	6.812135E-06	0.39699	H3SiO4-
4	1.248117E-02	0.94088	H4SiO4	4	1.248430E-02	0.94111	H4SiO4
5	9.583512E-34	0.94088	O2	5	1.626065E-36	0.94111	O2
6	7.042586E-06	0.94088	H2	6	1.709508E-04	0.94111	H2
7	4.440703E-03	0.94088	H2S	7	2.101150E-03	0.94111	H2S
8	7.249364E-05	0.34060	HS-	8	3.476620E-05	0.34106	HS-
9	2.722204E-11	0.02970	S2--	9	2.576762E-13	0.02980	S2--
10	4.082295E-08	0.02970	S2O3--	10	2.701727E-14	0.02980	S2O3--
11	5.887025E-07	0.94088	SO2	11	1.947043E-11	0.94111	SO2
12	5.532378E-11	0.02970	SO3--	12	1.878376E-15	0.02980	SO3--
13	6.489666E-07	0.36980	HSO3-	13	2.176388E-11	0.37023	HSO3-
14	1.061910E-03	0.02245	SO4--	14	1.484531E-09	0.02254	SO4--
15	2.801058E-04	0.39658	HSO4-	15	3.870392E-10	0.39699	HSO4-
16	1.458040E+00	0.30878	Cl-	16	1.457452E+00	0.30926	Cl-
17	2.265238E-04	0.94088	HCl	17	2.234509E-04	0.94111	HCl
18	9.976470E-01	0.36980	Na+	18	9.979242E-01	0.37023	Na+
19	1.453965E-05	0.94088	NaOH	19	1.477435E-05	0.94111	NaOH
20	1.398904E-03	0.39658	NaSO4-	20	1.964152E-09	0.39699	NaSO4-
21	4.669048E-01	0.30878	K+	21	4.594367E-01	0.30926	K+
22	2.775320E-06	0.94088	KOH	22	2.775320E-06	0.94111	KOH
23	2.692140E-03	0.39658	KSO4-	23	3.719893E-09	0.39699	KSO4-
24	5.052152E-05	0.94088	KHSO4	24	6.885351E-11	0.94111	KHSO4
25	1.031863E-15	0.00904	Al+++	25	9.845119E-16	0.00906	Al+++
26	3.181212E-11	0.02970	AlOH++	26	3.078623E-11	0.02980	AlOH++
27	1.149956E-08	0.39658	Al(OH)2+	27	1.132154E-08	0.39699	Al(OH)2+
28	1.231569E-06	0.94088	Al(OH)3	28	1.231569E-06	0.94111	Al(OH)3
29	1.103408E-06	0.39658	Al(OH)4-	29	1.118995E-06	0.39699	Al(OH)4-
30	4.414523E-50	0.00040	Au+++	30	3.506306E-52	0.00040	Au+++
31	1.148889E-28	0.39658	AuCl4-	31	9.225492E-31	0.39699	AuCl4-
32	1.029659E-05	0.05597	Fe++	32	2.888192E-05	0.05610	Fe++
33	1.326100E-06	0.39658	FeOH+	33	3.780186E-06	0.39699	FeOH+
34	2.605360E-08	0.94088	Fe(OH)2	34	7.543636E-08	0.94111	Fe(OH)2
35	6.431321E-12	0.39658	Fe(OH)3-	35	1.888449E-11	0.39699	Fe(OH)3-
36	5.963675E-06	0.94088	FeSO4	36	2.352706E-11	0.94111	FeSO4
37	1.665410E-05	0.39658	FeCl+	37	4.683024E-05	0.39699	FeCl+
38	4.433964E-06	0.94088	FeCl2	38	1.249228E-05	0.94111	FeCl2
39	5.744586E-17	0.00040	Fe+++	39	3.206834E-17	0.00040	Fe+++
40	3.014360E-12	0.02970	FeOH++	40	1.714577E-12	0.02980	FeOH++

41	2.095859E-08	0.39658	Fe(OH) 2+	41	1.212786E-08	0.39699	Fe(OH) 2+
42	3.550637E-07	0.94088	Fe(OH) 3	42	2.086913E-07	0.94111	Fe(OH) 3
43	2.885028E-10	0.39658	Fe(OH) 4-	43	1.719650E-10	0.39699	Fe(OH) 4-
44	2.510726E-15	0.02970	FeCl++	44	1.408736E-15	0.02980	FeCl++
<b>45</b>	<b>2.961353E-10</b>	<b>0.39658</b>	<b>AuCl2-</b>	<b>45</b>	<b>5.930550E-11</b>	<b>0.39699</b>	<b>AuCl2-</b>
<b>46</b>	<b>1.158459E-08</b>	<b>0.94088</b>	<b>AuOH</b>	<b>46</b>	<b>2.351023E-09</b>	<b>0.94111</b>	<b>AuOH</b>
<b>47</b>	<b>1.787787E-07</b>	<b>0.94088</b>	<b>AuHS</b>	<b>47</b>	<b>1.716710E-08</b>	<b>0.94111</b>	<b>AuHS</b>
<b>48</b>	<b>1.286764E-07</b>	<b>0.39658</b>	<b>Au(HS) 2-</b>	<b>48</b>	<b>5.928948E-09</b>	<b>0.39699</b>	<b>Au(HS) 2-</b>
49	5.016142E-01	0.94088	NaCl	49	5.027967E-01	0.94111	NaCl
50	4.099317E-02	0.94088	KCl	50	4.043709E-02	0.94111	KCl
I = 1.466				I = 1.458			
pH = 4.762				pH = 4.768			
Eh = -0.400				Eh = -0.479			

Bulk composition (mol)

Water 55.483474504

Al 2.345454E-06

Au 3.191923E-07

Cl 2.000000E+00

Fe 3.905923E-05

H 5.950807E-02

K 5.104139E-01

Na 1.500000E+00

O 7.191359E-02

S 1.000000E-02

Si 1.248228E-02

Options used: /i

Bulk composition (mol)

Water 55.481220240

Al 2.360759E-06

Au 2.549388E-08

Cl 2.000000E+00

Fe 9.223586E-05

H 5.479899E-02

K 4.996315E-01

Na 1.500000E+00

O 4.997538E-02

S 2.134906E-03

Si 1.248499E-02

Options used: /i

## REFERENCES

- Akinfiev, N. N. and Zotov, A. V. (2001). Thermodynamic description of chloride, hydrosulfide, and hydroxo complexes of Ag(I), Cu(I), and Au(I) at temperatures of 25-500°C and pressures of 1-2000 bar. *Geochemistry International* 39, 990–1006. <http://www.mai.ru/cgi-perl/search.pl?type=abstract&name=geochem&number=10&year=1&page=990>
- Akinfiev, N. N. and Zotov, A. V. (2010). Thermodynamic description of aqueous species in the system Cu-Ag-Au-S-O-H at temperatures of 0-600°C and pressures of 1-3000 bar. *Geochemistry International* 48, 714–720. [doi:10.1134/S0016702910070074](https://doi.org/10.1134/S0016702910070074)
- Caporuscio, F. A., Palaich, S. E. M., Cheshire, M. C., and Jové Colón, C. F. (2017). Corrosion of copper and authigenic sulfide mineral growth in hydrothermal bentonite experiments. *Journal of Nuclear Materials* 485, 137–146. [doi:10.1016/j.jnucmat.2016.12.036](https://doi.org/10.1016/j.jnucmat.2016.12.036)
- [Dataset] Dick, J. M. (2019). Code for the paper “CHNOSZ: Thermodynamic calculations and diagrams for geochemistry” (Version 2). Zenodo.org. <https://doi.org/10.5281/zenodo.2648521>
- Dick, J. M. and Shock, E. L. (2013). A metastable equilibrium model for the relative abundances of microbial phyla in a hot spring. *PLOS One* 8, e72395. [doi:10.1371/journal.pone.0072395](https://doi.org/10.1371/journal.pone.0072395)

- Helgeson, H. C. (1969). Thermodynamics of hydrothermal systems at elevated temperatures and pressures. *American Journal of Science* 267, 729–804. doi:10.2475/ajs.267.7.729
- Helgeson, H. C., Delany, J. M., Nesbitt, H. W., and Bird, D. K. (1978). Summary and critique of the thermodynamic properties of rock-forming minerals. *American Journal of Science* 278A, 1–229. <http://www.worldcat.org/oclc/13594862>
- Helgeson, H. C., Kirkham, D. H., and Flowers, G. C. (1981). Theoretical prediction of the thermodynamic behavior of aqueous electrolytes at high pressures and temperatures: IV. Calculation of activity coefficients, osmotic coefficients, and apparent molal and standard and relative partial molal properties to 600°C and 5 Kb. *American Journal of Science* 281, 1249–1516. doi:10.2475/ajs.281.10.1249
- Johnson, J. W., Oelkers, E. H., and Helgeson, H. C. (1992). SUPCRT92: A software package for calculating the standard molal thermodynamic properties of minerals, gases, aqueous species, and reactions from 1 to 5000 bar and 0 to 1000°C. *Computers & Geosciences* 18, 899–947. doi:10.1016/0098-3004(92)90029-Q
- Manning, C. E., Shock, E. L., and Sverjensky, D. A. (2013). The chemistry of carbon in aqueous fluids at crustal and upper-mantle conditions: Experimental and theoretical constraints. *Reviews in Mineralogy and Geochemistry* 75, 109–148. doi:10.2138/rmg.2013.75.5
- Pokrovski, G. S., Akinfiev, N. N., Borisova, A. Y., Zotov, A. V., and Kouzmanov, K. (2014). Gold speciation and transport in geological fluids: insights from experiments and physical-chemical modelling. *Geological Society, London, Special Publications* 402, 9–70. doi:10.1144/SP402.4
- Seewald, J. S. (1996). Mineral redox buffers and the stability of organic compounds under hydrothermal conditions. *Materials Research Society Symposium Proceedings* 432, 317–331. doi:10.1557/PROC-432-317
- Shock, E. L., Oelkers, E. H., Johnson, J. W., Sverjensky, D. A., and Helgeson, H. C. (1992). Calculation of the thermodynamic properties of aqueous species at high pressures and temperatures: Effective electrostatic radii, dissociation constants, and standard partial molal properties to 1000 °C and 5 kbar. *Journal of the Chemical Society, Faraday Transactions* 88, 803–826. doi:10.1039/FT9928800803
- Shvarov, Y. and Bastrakov, E. (1999). *HCh: A software package for geochemical equilibrium modelling. User's Guide*. Australian Geological Survey Organisation, Record 1999/25. <http://pid.geoscience.gov.au/dataset/ga/25473>
- Stumm, W. and Morgan, J. J. (1996). *Aquatic Chemistry: Chemical Equilibria and Rates in Natural Waters* (Wiley-Interscience), 3rd edn. <http://www.worldcat.org/oclc/974022850>
- Sverjensky, D. A., Shock, E. L., and Helgeson, H. C. (1997). Prediction of the thermodynamic properties of aqueous metal complexes to 1000°C and 5 kb. *Geochimica et Cosmochimica Acta* 61, 1359–1412. doi:10.1016/S0016-7037(97)00009-4
- Sverjensky, D. A., Stagno, V., and Huang, F. (2014). Important role for organic carbon in subduction-zone fluids in the deep carbon cycle. *Nature Geoscience* 7, 909–913. doi:10.1038/ngeo2291
- Williams-Jones, A. E., Bowell, R. J., and Migdisov, A. A. (2009). Gold in solution. *Elements* 5, 281–287. doi:10.2113/gselements.5.5.281